2016 ECORD Research Grant Final Report

Rupture to the trench? Frictional properties of accretionary wedge sediments at the Cascadia margin

Caroline Seyler, Dept. of Earth & Planetary Sciences, McGill University

Email: caroline.seyler@mail.mcgill.ca

1. Introduction

Subduction zone faults host the world's largest earthquakes and account for approximately 90% of the total seismic moment released globally in the 20th century (Pacheco and Sykes, 1992), constituting a major natural hazard to populations worldwide. During a megathrust earthquake, large amounts of slip on the shallow segment of subduction zone faults promote the generation of tsunami waves, as seen in the 2004 Sumatra and 2011 Tohoku-Oki earthquakes (Ide et al., 2011; Lay et al., 2005). Paleoseismic studies for the Cascadia subduction zone reveal a history of large magnitude, tsunamigenic earthquakes (Goldfinger et al., 2012; Leonard et al., 2010). Since the last M_w 9 event in 1700 A.D. (Satake et al., 2003), the Cascadia subduction zone has been accumulating elastic strain to be released in a future megathrust earthquake (Dragert et al., 1994; Savage et al., 1981). A large magnitude event today would produce devastating releases of seismic energy and potentially trigger tsunami waves, resulting in billions of dollars of damage and thousands of fatalities (Cascadia Region Earthquake Workgroup, 2013). Given the probability of another large magnitude earthquake at Cascadia, what is the likelihood of earthquake rupture propagation to the trench?

Friction is the primary control on coseismic slip distribution, so determining the frictional properties of the shallow subduction fault is essential to providing constraints for rupture modeling and evaluating seismic and tsunami hazard (Noda and Lapusta, 2013). Shallow coseismic slip on subduction zone faults requires rupture through predominantly clay-rich sediments in the accretionary prism, which are observed to localize deformation at multiple margins (Moore, 1989). The frictional properties of these clay-rich layers will thus control slip behavior on the shallow subduction thrust (Faulkner et al., 2011; Kameda et al., 2015; Oohashi et al., 2015). Experiments on clay-rich sediments at low (~μm/s) sliding velocities often exhibit low coefficients of friction ($\mu < 0.4$), which enhances localization and stable, rate-strengthening behavior, inhibiting earthquake nucleation (Ikari et al., 2015; Ikari et al., 2009; Saffer and Marone, 2003). At high (~m/s) sliding velocities, clay-rich sediments rapidly weaken with slip and demonstrate anomalously low fracture energy, a mechanical property that dictates the relative difficulty of rupture propagation (Di Toro et al., 2011; Remitti et al., 2015; Sawai et al., 2014; Ujiie et al., 2013). Further, these low and high velocity properties vary with clay species and quartz content, with smectite exhibiting the lowest coefficient of friction at low sliding velocities (μ = 0.15-0.32

at 0.1 to 200 μm/s) and velocity weakening behavior at low normal stress (Saffer and Marone, 2003).

To-date, there has been no experimental work measuring frictional properties of the Cascadia subduction zone. This project explores the effects of lithology and pore pressure on the frictional strength and stability of the shallow subduction zone fault at Cascadia by conducting low velocity friction experiments. Here, I present initial results of low velocity friction experiments on ocean drill core samples of sedimentary rocks from the Juan de Fuca plate that comprise the input to the Cascadia subduction zone.

2. Materials and methods

2.1 Core samples

Core samples were obtained from two Ocean Drilling Program (ODP) sites adjacent to the Cascadia margin: Site 1027 of Expedition 168 and Site 888 of Expedition 146 (Fig. 1A). These sites successfully capture the lithologic variation throughout the stratigraphic section and underlying basalt basement. The oceanic stratigraphy is dominated by clay-rich rocks, including turbidites, massively bedded clays, silt, and fine sand, and hemipelagic mudstones (Fig. 1B) (Carson et al., 1995; Fisher et al., 2000; Westbrook et al., 1994). Three similar stratigraphic units have been identified at both sites, with one additional unit present at Site 1027 (Carson et al., 1995; Fisher et al., 2000; Westbrook et al., 1994). Clay content varies with each lithology, with smectite, illite, chlorite, and kaolinite previously reported at Site 1027 (Fisher et al., 2000). For the friction experiments, samples from the four lithologic units were selected to represent the input section to the Cascadia subduction zone (Table 1).

Table 1: Summary of selected core samples from ODP Sites 1027 and 888

Lithology	Core samples	Units
1. Turbidites, clay, silt, and interbedded sands	168-1027B-03H-3	Site 1027: Unit Ia
	146-888B-14H-3	Site 888: Unit I
2. Massively bedded clays, silt, and fine sand	168-1027B-25X-2	Site 1027: Unit Ib
	146-888B-25H-2	Site 888: Unit II
3. Hemipelagic mud	168-1027B-53X-2	Site 1027: Unit II
	146-888B-62X-2	Site 888: Unit III
4. Indurated mudstone and carbonate-rich claystone	168-1027C-02R-3	Site 1027: Unit III

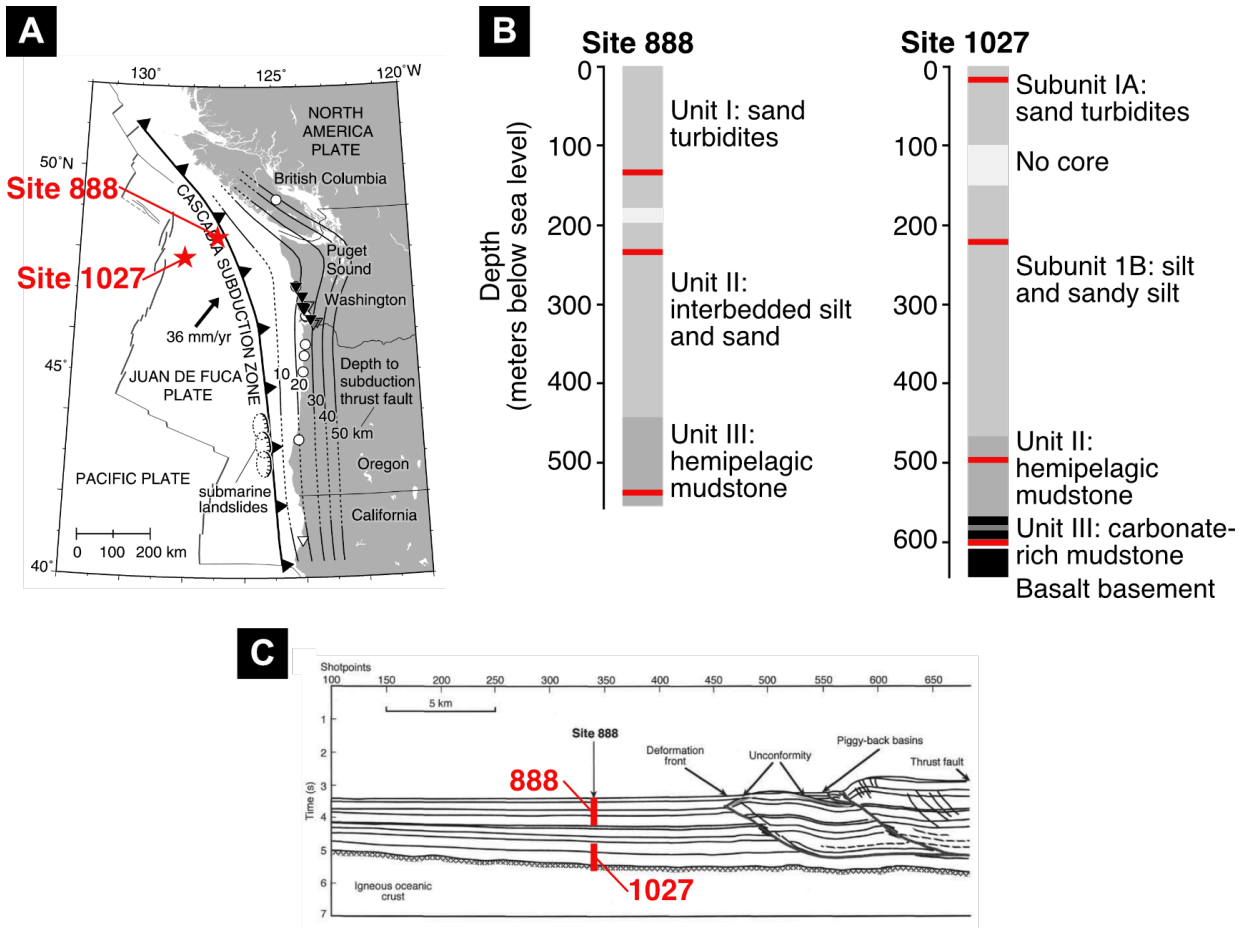

Figure 1: Location of core samples
A) Locations of IODP sites (red stars) relative to the Cascadia subduction zone, note the sites are effectively in a transect parallel to the plate convergence direction; B) Schematic stratigraphy at IODP sites with core samples selected for experiments highlighted with red bars; C) Interpretative sketch of seismic reflection data showing the relative depth of stratigraphy in each hole (actual depth of Site 888 and equivalent depth of Site 1027) (figure adapted from Fisher et al. (2000), Satake et al. (2003), and Westbrook et al. (1994)).

2.2 X-ray diffraction

Sample mineralogy and dominant clay species of the selected core samples were characterized using x-ray diffraction (XRD) data from whole rock analysis and clay separate analysis. The samples were ground into <90 μm powders with an alumina mortar and pestle followed by the McCrone micronizing mill. Randomly oriented whole rock powder and oriented clay mounts were prepared following the methods set forth by the USGS laboratory manual for XRD (Poppe et al., 2001) to assure meaningful results. Samples were analyzed in a Rigaku SmartLab® high resolution x-ray diffractometer with Cu Ka radiation. Oriented clay mounts were analyzed untreated, expanded with ethylene glycol, and heated to 400 ˚C to test for any expansion or destruction of the clay crystal structure.

2.3 Friction experiments

I conducted friction experiments in the triaxial deformation apparatus in the Rock and Ice Mechanics Lab at Lamont-Doherty Earth Observatory (Fig. 2). Initial experiments were conducted with a 45˚ shear piston geometry at room temperature with hydrostatic pore pressure and confining pressures of 40 to 100 MPa. Gouge was synthesized by mixing 10 mL of sample powder with 2 mL of DI water or sea water. Samples were powdered by grinding the core material in an alumina mortar and pestle and sieved to <250 μm. During each experiment, a series of velocity steps and slide-hold-slide tests measured the frictional response of the deforming material. Half-order and order of magnitude velocity steps between 1, 3, and 10 μm/s measured the velocity-dependence of friction and stability, and slide-hold-slide tests with holds of 1, 10, 100, and 1,000 seconds between periods of sliding at 1 μm/s measured the amount of healing.

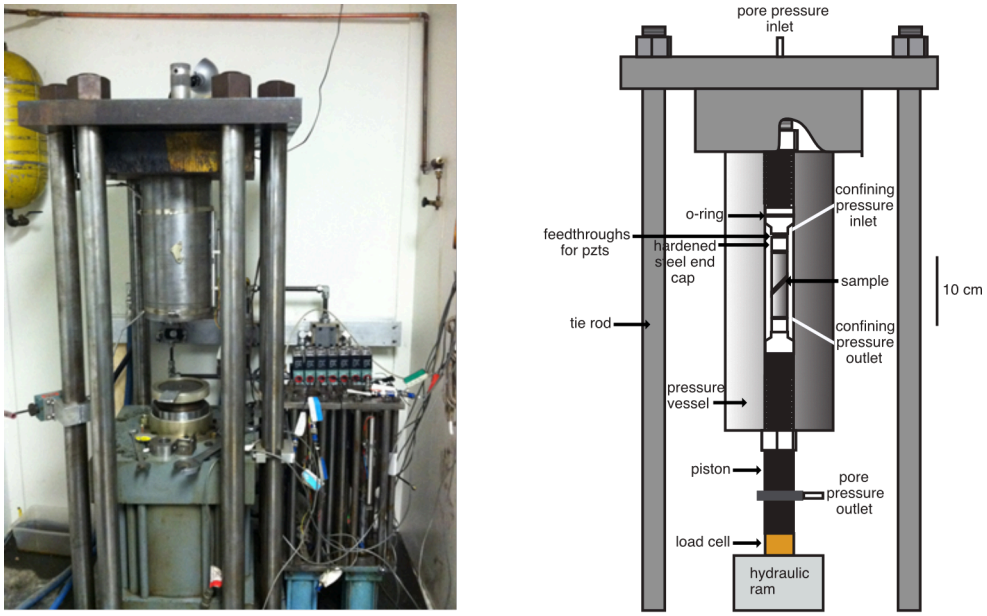

Figure 2: Triaxial deformation apparatus
Triaxial deformation apparatus and sample assembly in the Rock and Ice Mechanics lab at the Lamont-Doherty Earth Observatory.

3. Initial results and discussion

3.1 Mineralogy

Lithologic variations in mineral assemblages between the core samples are limited, but the relative abundance of quartz, feldspar, and clays is somewhat variable. Whole rock and oriented clay separate XRD spectra for all samples are plotted in Fig. 3 and Fig. 4, respectively. All samples have prominent quartz peaks at ~26 ˚ 2θ and ~50˚ 2θ in the whole rock XRD spectra. Mineralogy was quantified using Rietveld refinement, and the modal abundances of phases are reported in Table 2.

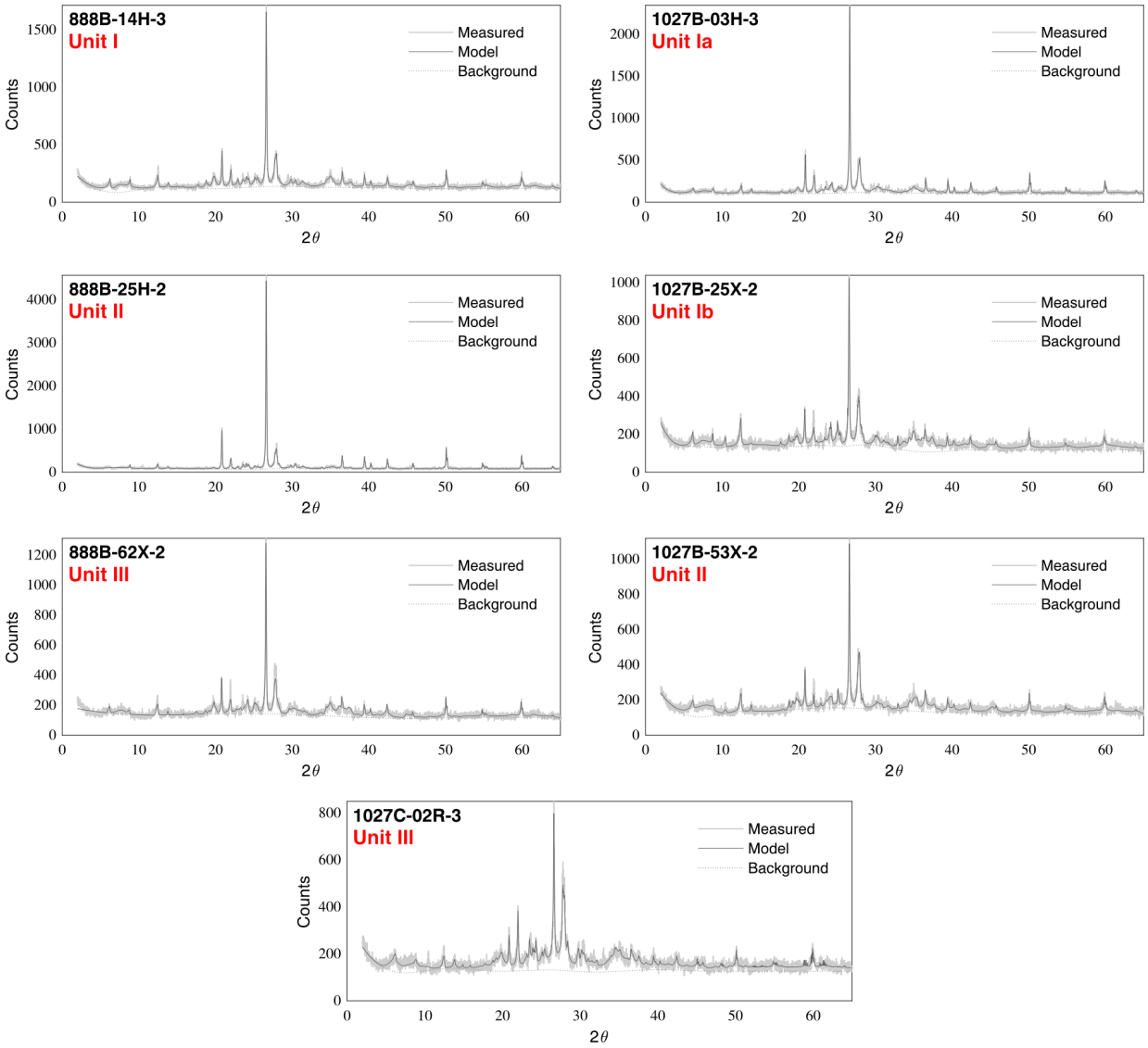

Figure 3: Whole rock XRD spectra

XRD spectra from randomly oriented whole rock powder analyses for the selected core samples. The observed spectra (light grey), model fit (dark grey), and background (dotted line) are plotted for each sample.

Table 2: Mineralogy of core samples determined from XRD

Sample	Qz	Fsp	Ilt	Chl	Mnt	Amp	Cal	Py
888B-14H-3	24%	26%	26%	15%	8%	-	-	-
888B-25H-2	47%	36%	11%	6%	-	-	-	-
888B-62X-2	24%	40%	26%	8%	<5%	-	-	-
1027B-03H-3	31%	41%	20%	8%	<5%	-	-	-
1027B-25X-2	19%	39%	16%	19%	<5%	5%	-	-
1027B-53X-2	25%	20%	25%	19%	9%	<5%	-	-
1027C-02R-3	<5%	26%	39%	<5%	<5%	10%	<5%	11%

All samples contain quartz, feldspar, and clay minerals, with some samples at Site 1027 also containing small amounts of amphibole, calcite, and pyrite. Diagnostic clay peaks appear in the whole rock XRD spectra at <20˚ 2θ, corresponding to large d-spacing values. Chlorite, illite, and montmorillonite are present in nearly all seven samples. These clay minerals were identified by observing diagnostic peaks in the clay separate spectra, which correspond to d-spacing in the clay mineral structure. Montmorillonite has a peak at ~15.1 Å that expands to ~18.2 Å when glycolated and collapses back to ~15.1 Å when heated to 400 ˚C. Illite has diagnostic peaks at ~10.3 Å and ~5.0 Å, and chlorite has diagnostic peaks at ~7.3 Å and ~4.8 Å. Illite and chlorite peaks are unaffected by the ethylene glycol and heat treatments.

Overall, the samples are dominated by quartz, feldspar, and clay minerals, with the total phyllosilicate content ranging from 17% to 49% at Site 888 and 29% to 52% at Site 1027. These results are consistent with the mineralogy reported in the IODP proceedings for Expeditions 146 and 168.

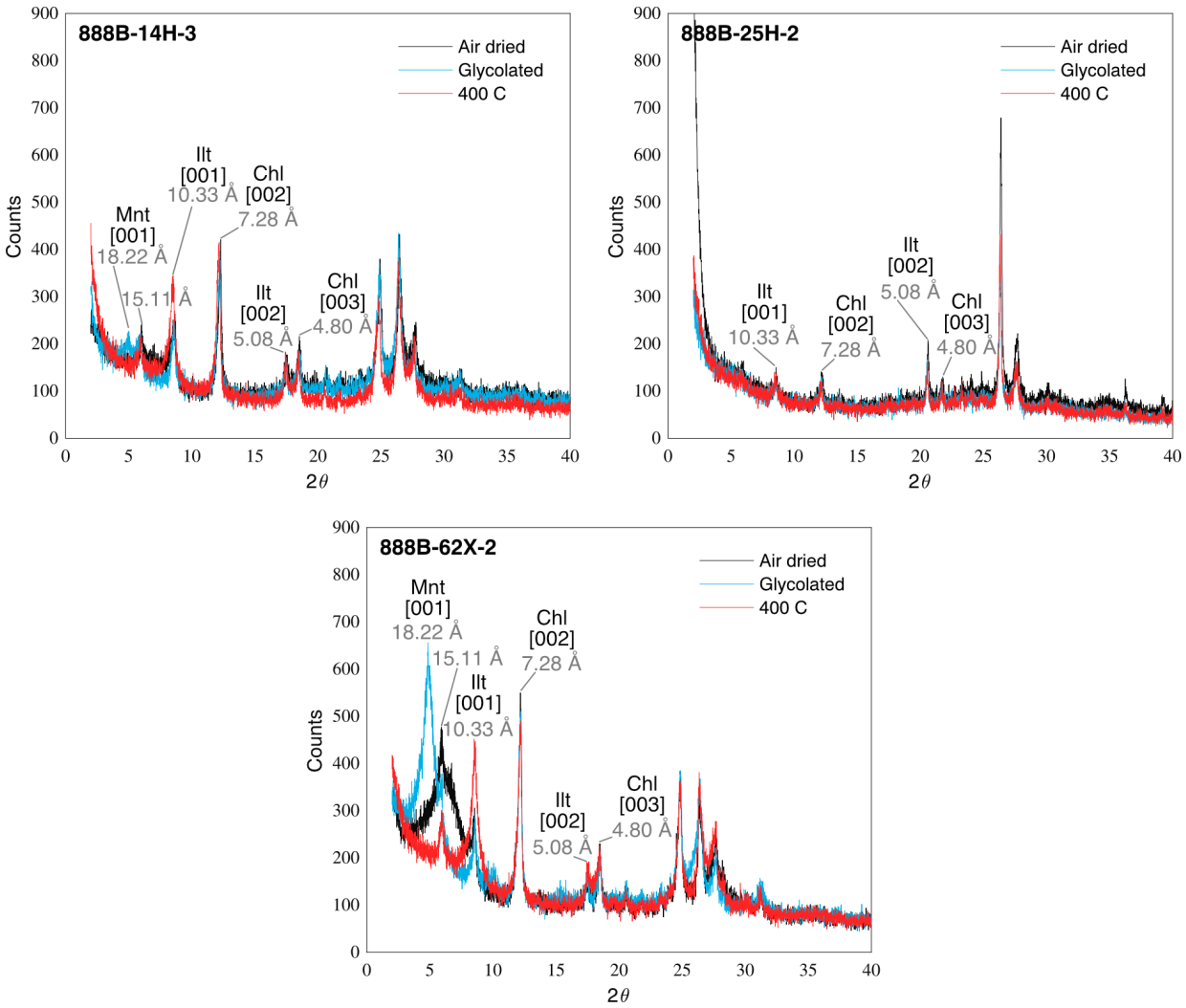

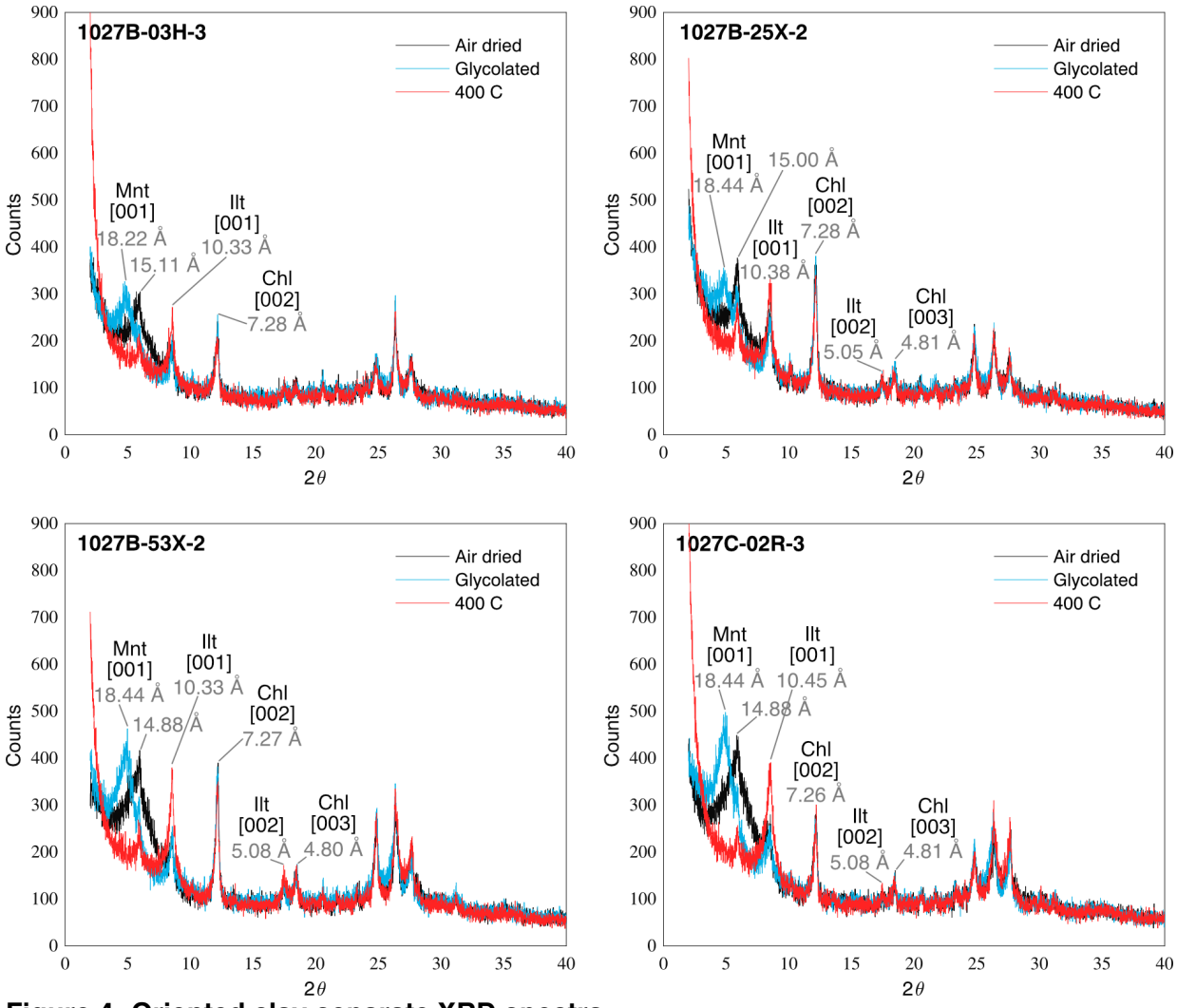

Figure 4: Oriented clay separate XRD spectra

XRD spectra from oriented clay separate analyses for the selected core samples. Measurement data for the air dried (black), glycolated (blue), and heat treated (red) analyses are plotted for each sample. Diagnostic peaks are labelled by d-spacing and identified clay mineral. Mnt—montmorillonite; Ilt—illite; Chl—chlorite.

3.2 Mechanical data

Friction experiments conducted on three core samples are detailed in Table 2. The coefficient of friction is measured as the ratio of effective normal stress to shear stress resolved on the 45° dipping interface. Mechanical data indicates a moderately high coefficient of friction for sample 888B-25H-2, a moderately low coefficient of friction for sample 1027B-53X-2, and an extremely low coefficient of friction for sample 1027C-02R-3 (Fig. 5A). Mohr-Coulomb failure envelopes were constructed by measuring shear stress at multiple effective normal stresses for each sample, with the slope of the failure envelope approximating the steady state friction coefficient (Fig. 5B). These results are consistent with the expected frictional behavior based on the observed mineralogy, with the quartz- and feldspar-rich sample (888B-25H-2) demonstrating a higher coefficient of

friction (μ ~ 0.66) than the clay-dominated samples (μ ~ 0.3-0.4). The extremely low coefficient of friction (μ ~ 0.1) in sample 1027C-02R-3 is likely related to pore fluid overpressure due to low permeability in the sample. The low coefficient of friction in the clay-rich samples highlights the potential for localization into anomalously weak layers within the input section, and the possibility of trench-ward rupture along the shallow subduction zone fault at Cascadia.

Table 3: Summary of friction experiments

Expt. No.	Sample	Pore fluid	Pc (MPa)	Pp (MPa)	μ_{ss}
T007	1027B-53X-2	DI water N/A	50, 60, 70, 80, 90, 100	0	0.38
T009	1027B-53X-2	Sea water Hydrostatic	40, 70, 100	20, 35, 50	0.43
T010	1027C-02R-3	Sea water Hydrostatic	40, 70	25, 35	0.33
T011	888B-25H-2	Sea water Hydrostatic	40, 70	25, 35	0.66

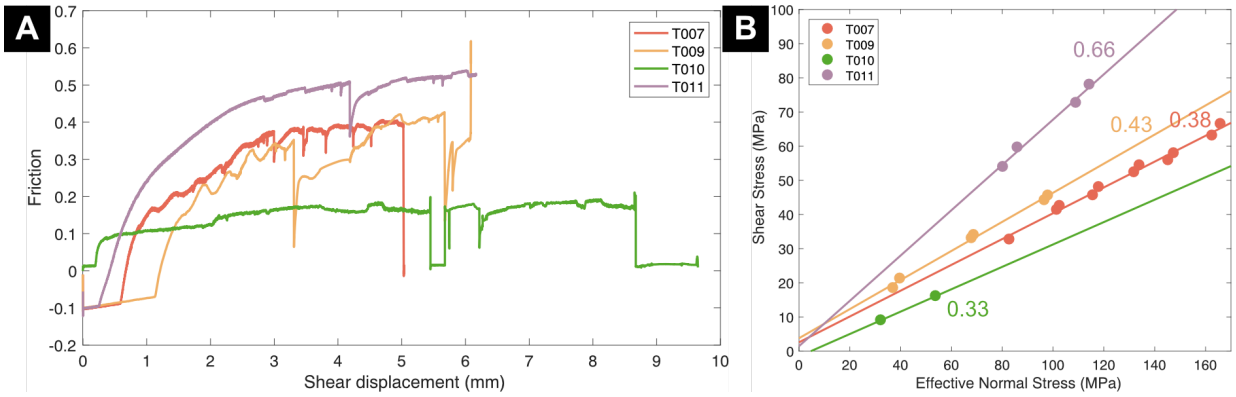

Figure 5: Friction
Friction results for four experiments on variable lithologies. A) Shear displacement vs. coefficient of friction experiment curves; B) Mohr-Coulomb failure envelopes; slope estimates the steady-state coefficient of friction for each experiment.

4. Future work

Further work will:

- Complete a suite of high temperature low velocity experiments (~250 ˚C)
- Evaluate the frictional stability of the core samples with rate-and-state
- Prepare post-experiment thin sections and review deformation-related microstructures, including deformation fabrics, fault geometry, and localization features

5. Final budget

Date	Item	Cost (Euros)
26-Sept-2016	Pre-experiment thin sections (CAD$817.97)	€556.22
11-Nov-2016	Return flight to New York (CAD$386.30)	€262.68
27-Nov-2016	Return travel to Trudeau Airport in Montréal (CAD$20)	€13.60
27-Nov-2016	Travel from LaGuardia Airport to LDEO (US$145.30)	€130.77
03-Dec-2016	Subsistence in New York (CAD$126)	€85.68
Feb-April 2017	X-ray diffraction analysis (CAD$2,200.00)	€1,496.00

6. Acknowledgements

I am grateful to ECORD and the ESSAC Science Committee for their financial support. I would like to thank Dr. James Kirkpatrick at McGill and Dr. Heather Savage at LDEO for supporting this proposal and scientific discussions regarding this research, Hannah Rabinowitz and Ted Koczynski at the LDEO Rock and Ice Mechanics lab for their help with sample assembly and conducting friction experiments, and Dr. Christie Rowe at McGill University for facilitating XRD analysis. Samples were provided by the International Ocean Discovery Program (IODP).

7. References

Carson, B., Westbrook, G. K., Musgrave, R. J., and Suess, E., 1995, Proceedings of the Ocean Drilling Program, Scientific Results, Vol.146 (Part 1): Ocean Drilling Program.

Cascadia Region Earthquake Workgroup, 2013, Cascadia Subduction Zone Earthquakes: A Magnitude 9.0 Earthquake Scenario.

Di Toro, G., Han, R., Hirose, T., De Paola, N., Nielsen, S., Mizoguchi, K., Ferri, F., Cocco, M., and Shimamoto, T., 2011, Fault lubrication during earthquakes: Nature, v. 471, no. 7339, p. 494-498.

Dragert, H., Hyndman, R., Rogers, C., and Wang, K., 1994, Current deformation and the with of the seismogenic zone of the northern Cascadia subduction thrust: Journal of Geophysical Research: Solid Earth, v. 99, no. B1, p. 653-668.

Faulkner, D. R., Mitchell, T. M., Behnsen, J., Hirose, T., and Shimamoto, T., 2011, Stuck in the mud? Earthquake nucleation and propagation through accretionary forearcs: Geophysical Research Letters, v. 38, no. 18, p. 1-5.

Fisher, A., Davis, E. E., and Escutia, C., 2000, Proceedings of the Ocean Drilling Program, Scientific Results, Vol.168: Ocean Drilling Program.

Goldfinger, C., Nelson, C. H., Morey, A. E., Johnson, J. E., Patton, J. R., Karabanov, E., Gutierrez-Pastor, J., Eriksson, A., Gracia, E., Dunhill, G., Enkin, R., Dallimore, A., and Vallier, T., 2012, Turbidite Event History - Methods and Implications for Holocene Paleoseismicity of the Cascadia Subduction Zone: U.S. Geological Survey.

Ide, S., Baltay, A., and Beroza, G. C., 2011, Shallow dynamic overshoot and energetic deep rupture in the 2011 Mw 9.0 Tohoku-Oki earthquake: Science, v. 332, no. 6036, p. 1426-1429.

Ikari, M. J., Kameda, J., Saffer, D. M., and Kopf, A. J., 2015, Strength characteristics of Japan Trench borehole samples in the high-slip region of the 2011 Tohoku-Oki earthquake: Earth and Planetary Science Letters, v. 412, p. 35-41.

Ikari, M. J., Saffer, D. M., and Marone, C., 2009, Frictional and hydrologic properties of clay-rich fault gouge: Journal of Geophysical Research: Solid Earth, v. 114, no. B5, p. B05409.

Kameda, J., Shimizu, M., Ujiie, K., Hirose, T., Ikari, M., Mori, J., Oohashi, K., and Kimura, G., 2015, Pelagic smectite as an important factor in tsunamigenic slip along the Japan Trench: Geology, v. 43, no. 2, p. 155-158.

Lay, T., Kanamori, H., Ammon, C. J., Nettles, M., Ward, S. N., Aster, R. C., Beck, S. L., Bilek, S. L., Brudzinski, M. R., Butler, R., DeShon, H. R., Ekström, G., Satake, K., and Sipkin, S., 2005, The Great Sumatra-Anadaman Earthquake of 26 December 2004: Science, v. 308, no. 5725, p. 1127-1133.

Leonard, L. J., Currie, C. A., Mazzotti, S., and Hyndman, R. D., 2010, Rupture area and displacement of past Cascadia great earthquakes from coastal coseismic subsidence: Geological Society of America Bulletin, v. 122, no. 11-12, p. 2079-2096.

Moore, J. C., 1989, Tectonics and hydrogeology of accretionary prisms: role of the décollement zone: Journal of Structural Geology, v. 11, no. 1-2, p. 95-106.

Noda, H., and Lapusta, N., 2013, Stable creeping fault segments can become destructive as a result of dynamic weakening: Nature, v. 493, no. 7433, p. 518-521.

Oohashi, K., Hirose, T., Takahashi, M., and Tanikawa, W., 2015, Dynamic weakening of smectite-bearing faults at intermediate velocities: Implications for subduction zone earthquakes: Journal of Geophysical Research: Solid Earth, v. 120, no. 3, p. 1572-1586.

Pacheco, J. F., and Sykes, L. R., 1992, Seismic moment catalog of large shallow earthquakes, 1900 to 1989: Bulletin of the Seismological Society of America, v. 82, no. 3, p. 1306-1349.

Poppe, L. J., Paskevich, V. F., Hathaway, J. C., and Blackwood, D. S., 2001, A laboratory manual for X-ray powder diffraction: U.S. Geological Survey.

Remitti, F., Smith, S. A. F., Mittempergher, S., Gualtieri, A. F., and Di Toro, G., 2015, Frictional properties of fault zone gouges from the J-FAST drilling project (Mw 9.0 2011 Tohoku-Oki earthquake): Geophysical Research Letters, v. 42, no. 8, p. 2691-2699.

Saffer, D. M., and Marone, C., 2003, Comparison of smectite- and illite-rich gouge frictional properties: application to the updip limit of the seismogenic zone along subduction megathrusts: Earth and Planetary Science Letters, v. 215, no. 1-2, p. 219-235.

Satake, K., Wang, K., and Atwater, B. F., 2003, Fault slip and seismic moment of the 1700 Cascadia earthquake inferred from Japanese tsunami descriptions: Journal of Geophysical Research: Solid Earth, v. 108, no. B11, p. 2535.

Savage, J. C., Lisowski, M., and Prescott, W. H., 1981, Geodetic strain measurements in Washington: Journal of Geophysical Research: Solid Earth, v. 86, no. B6, p. 4929-4940.

Sawai, M., Hirose, T., and Kameda, J., 2014, Frictional properties of incoming pelagic sediments at the Japan Trench: implications for large slip at a shallow plate boundary during the 2011 Tohoku earthquake: Earth, Planets and Space, v. 66, no. 1, p. 65-65.

Ujiie, K., Tanaka, H., Saito, T., Tsutsumi, A., Mori, J. J., Toczko, S., and Scientists, E. a. T., 2013, Low coseismic shear stress on the Tohoku-Oki megathrust determined from laboratory experiments: Science, v. 342, no. 6163, p. 1211-1214.

Westbrook, G. K., Carlson, B., and Musgrave, R. J., 1994, Proceedings of the Ocean Drilling Program, Initial Reports, Vol.146: Ocean Drilling Program.